Journal of Power Sources 198 (2012) 258–263

Contents lists available at SciVerse ScienceDirect

Journal of Power Sources

journal homepage: www.elsevier.com/locate/jpowsour

Synthesis and electrochemical properties of $LiNi_{0.8}Co_{0.15}Al_{0.05}O_2$ prepared from the precursor $Ni_{0.8}Co_{0.15}Al_{0.05}OOH$

Guorong Hu[a], Wanmin Liu[a,b,*], Zhongdong Peng[a], Ke Du[a], Yanbing Cao[a]

[a] School of Metallurgical Science and Engineering, Central South University, Changsha 410083, China
[b] School of Chemistry and Chemical Engineering, Hunan Institute of Engineering, Xiangtan 411104, China

ARTICLE INFO

Article history:
Received 17 July 2011
Received in revised form
29 September 2011
Accepted 29 September 2011
Available online 5 October 2011

Keywords:
Lithium-ion battery
Cathode material
Co-oxidation-controlled crystallization
Electrochemical property

ABSTRACT

$LiNi_{0.8}Co_{0.15}Al_{0.05}O_2$ cathode material for lithium-ion batteries is synthesized by sintering the precursor $Ni_{0.8}Co_{0.15}Al_{0.05}OOH$, which is prepared from the corresponding metal sulphates solution by a co-oxidation-controlled crystallization method. The effects of calcination temperature and time on the electrochemical performance of the material are investigated on the basis of TG-DSC analysis. XRD analyses show that the powders obtained by calcination at 700 °C for 6 h have the best-ordered hexagonal layer structure. SEM images show that these powders are spherical particles with diameter in the 5–12 μm range. The XPS measurement and the chemical titration display that Ni ions of these powders are in the form of Ni^{3+}. The charge–discharge tests demonstrate that these powders have the best electrochemical properties, with an initial discharge capacity of 196.8 mAh g^{-1} and capacity retention of 96.1% after 50 cycles when cycled at a current density of 0.2 C between 2.8 and 4.3 V. Besides, these powders have also exhibited excellent rate capability and high-temperature performance.

1. Introduction

$LiNiO_2$ is considered as a very promising cathode material for lithium-ion batteries due to its low cost and high specific capacity [1,2]. However, it has several problems, such as difficult synthesis, low thermal stability, and poor cycle life in the charged state [3–5]. It has been known that the cationic substitution in $LiNiO_2$ is one of the important methods to improve electrochemical reactivity. Among them, Co and Al co-doped $LiNiO_2$-based materials are one of the most applicable materials due to the relatively good thermal stability and cyclability [6–11]. Recently, $LiNi_{0.8}Co_{0.15}Al_{0.05}O_2$ powders were prepared by various synthesis methods, such as co-precipitation [12], sol–gel synthesis [13], solution combustion route [14], PVA precursor method [15] and spray pyrolysis method [16]. Among all of these methods, nickel ions of the precursors existed entirely in the form of Ni^{2+}. It is well-known that Ni^{2+} is oxidized completely to Ni^{3+} with difficulty even at high temperature under flowing oxygen [17–19], which eventually leads to a lithium deficient material due to the cation disorder of remnant divalent nickel ions in the lithium site when $y \leq 0.2$ in the $LiNi_{1-y}M_yO_2$ phases (where M is a transition metal), in spite of the existence of dopants such as trivalent cobalt ions and aluminum ions [20–23]. Further, the existence of lithium deficiency in the material strongly affects the structural and electrochemical properties. Thus, it remains a major challenge to prepare the nickel-rich based cathode material with high discharge capacity and good cycle life.

In this paper, in attempt to reduce cation mixing and improve the electrochemical properties of $LiNi_{0.8}Co_{0.15}Al_{0.05}O_2$ cathode, the precursor $Ni_{0.8}Co_{0.15}Al_{0.05}OOH$ with the mixture of three trivalent metal cations at the atom level was prepared by a co-oxidation-controlled crystallization method, then the precursor was mixed with lithium source and sintered at high temperature, the spherical powder $LiNi_{0.8}Co_{0.15}Al_{0.05}O_2$ was obtained.

2. Experimental

A black spherical $Ni_{0.8}Co_{0.15}Al_{0.05}OOH$ precursor was prepared by the co-oxidation-controlled crystallization method described in our previous report [24]. During the course of the precursor preparation, the pH value and temperature were strictly controlled at 10.5 ± 0.2 and 50 °C, respectively. The dried precursor was then ground with an excess of $LiOH{\cdot}H_2O$ (Li/(Ni + Co + Al) = 1.06) and sintered at different temperatures for different time in flowing oxygen to obtain $LiNi_{0.8}Co_{0.15}Al_{0.05}O_2$ powders.

Thermal decomposition behavior of the mixture of $Ni_{0.8}Co_{0.15}Al_{0.05}OOH$ and $LiOH{\cdot}H_2O$ was examined by thermogravimetric and differential scanning calorimeter (TG/DSC, NETZSCH STA 449C) between 30 and 1000 °C at a heating rate of 10 °C min^{-1} under flowing oxygen. The structure of the powders

* Corresponding author. Tel.: +86 731 88830474; fax: +86 731 88830474.
E-mail address: mwliu22@yahoo.com.cn (W. Liu).

0378-7753/$ – see front matter © 2011 Elsevier B.V. All rights reserved.
doi:10.1016/j.jpowsour.2011.09.101

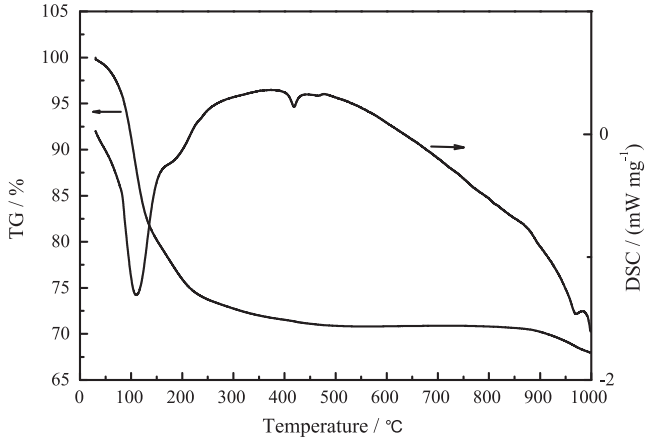

Fig. 1. TG/DSC curves of the mixture of $Ni_{0.8}Co_{0.15}Al_{0.05}OOH$ and $LiOH{\cdot}H_2O$.

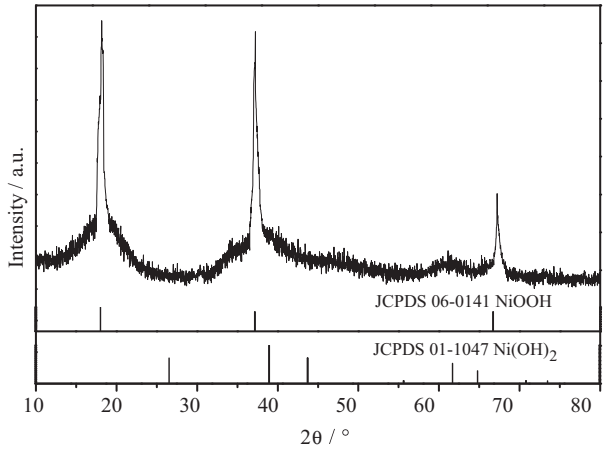

Fig. 2. The XRD pattern of $Ni_{0.8}Co_{0.15}Al_{0.05}OOH$ prepared by the co-oxidation-controlled crystallization method.

was determined by X-ray diffraction (XRD, D/max-r A type Cu Kα, 40 kV, 300 mA, 10–80 °C). The particle morphology of the products was observed by means of scanning electron microscopy (SEM, JEOL JSM-6360LV). The concentration of lithium, nickel, cobalt, aluminum, etc. of the products was measured by inductively coupled plasma atomic emission spectroscopy (ICP-AES, Optima 4300DV). The oxidation state of nickel of the products was analyzed by the chemical titration [18] in Ar atmosphere and X-ray photoelectron spectroscopy (XPS, K-Alpha 1063).

The electrochemical characteristics of the synthesized cathode powders were carried out using a two-electrode test cell with lithium foil as the negative electrode. A positive electrode was made by coating a paste of $LiNi_{0.8}Co_{0.15}Al_{0.05}O_2$ active material, acetylene black and polyvinylidene fluoride (PVDF) binder (in the weight ratio of 80:10:10) on an aluminum-foil collector, with N-methylpyrrolidone (NMP) as the solvent. The positive film was subjected to roll press and the electrodes of 10 mm diameter were punched out. The positive electrodes were then dried at 120 °C for 12 h in a vacuum oven. The coin-type cells (CR 2032) were assembled in an argon filled glove box with an electrolyte of 1 mol L^{-1} $LiPF_6$ in EC-DMC-EMC (1:1:1, volume ratio) solution and a separator of Celgard 2400. The charge–discharge measurements were performed at a current density of 0.2 C within the voltage range of 2.8–4.3 V on a battery test system (LAND CT2001A, Land Co., China).

3. Results and discussion

3.1. Thermal analysis

Fig. 1 shows the TG and DSC curves of the mixture of $Ni_{0.8}Co_{0.15}Al_{0.05}OOH$ and $LiOH{\cdot}H_2O$ under flowing oxygen. The TG curve displays that weight loss takes place in several steps. The first weight loss step between 30 and 150 °C is ascribed to the removal of adsorbed water in the precursor powders and crystal water of $LiOH{\cdot}H_2O$ with 20.8% weight loss. The second step of 5.3% weight loss, which occurs between 150 and 275 °C, is ascribed to the decomposition of $Ni_{0.8}Co_{0.15}Al_{0.05}OOH$, corresponding to an endothermic peak at about 180 °C in DSC curve. The third step of 2.7% weight loss between 275 and 500 °C is attributed to the decomposition of LiOH. During this course, LiOH melted and subsequently decomposed, and it is evidenced by an obvious endothermic peak at 418.7 °C in DSC curve. Around 500 °C, the active reaction takes place and the precursor starts to form the layered compound. In the temperature range of higher than 800 °C, there is a continuous weight loss process, which is attributed to part decomposition of the as-formed crystalline because of the loss of oxygen and lithium [25–27]. These facts indicate that the final product can be obtained at a temperature range of 500–800 °C. Therefore, the selected heating treatment process is that, firstly, at 450 °C for 3 h, LiOH is ensured to melt and coat on the surface of the decomposed precursor, then $LiNi_{0.8}Co_{0.15}Al_{0.05}O_2$ powders are synthesized at elevated temperature in flowing oxygen.

3.2. XRD studies

Fig. 2 presents the XRD pattern of $Ni_{0.8}Co_{0.15}Al_{0.05}OOH$ precursor prepared by the co-oxidation-controlled crystallization method. It can be seen that the diffraction peak positions of the precursor deviate slightly from that of NiOOH due to the difference of three metal ionic radii. Moreover, the diffraction peaks of $Ni(OH)_2$ cannot be found in the XRD pattern. This indicates that the precursor may be $Ni_{0.8}Co_{0.15}Al_{0.05}OOH$.

Fig. 3 displays the XRD patterns of the $LiNi_{0.8}Co_{0.15}Al_{0.05}O_2$ samples sintered at different temperatures for 6 h. As can be seen, these samples fit well with α-$NaFeO_2$ structure. However, the diffraction peaks are broad for the sample calcined at 600 °C, indicating the crystallization is incomplete at this temperature. As the temperature increases, all the peaks in the patterns become sharper and stronger, indicating the improved crystallinity of the materials with increasing calcination temperatures. This is also confirmed by the splitting degree of the hexagonal doublets (0 0 6)/(0 1 2) and

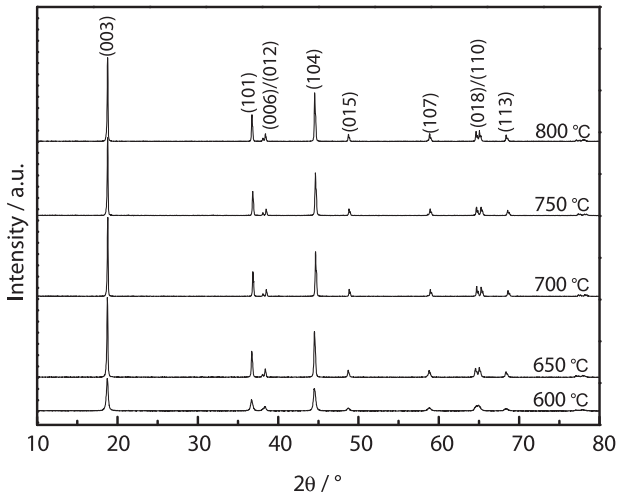

Fig. 3. XRD patterns of the $LiNi_{0.8}Co_{0.15}Al_{0.05}O_2$ samples sintered at various temperatures for 6 h.

Table 1
Structural and lattice parameters of $LiNi_{0.8}Co_{0.15}Al_{0.05}O_2$ samples sintered at various temperatures and time.

Reaction conditions	a (±0.0003 Å)	c (±0.0004 Å)	c/a	$I_{(0\,0\,3)}/I_{(1\,0\,4)}$	R-factor
600 °C, 6 h	2.872	14.194	4.94	1.23	0.45
650 °C, 6 h	2.866	14.180	4.95	1.29	0.40
700 °C, 6 h	2.857	14.168	4.96	1.34	0.36
750 °C, 6 h	2.858	14.162	4.96	1.33	0.37
800 °C, 6 h	2.866	14.159	4.94	1.31	0.42
700 °C, 3 h	2.874	14.186	4.94	1.13	0.53
700 °C, 6 h	2.857	14.168	4.96	1.34	0.36
700 °C, 10 h	2.856	14.160	4.96	1.33	0.38
700 °C, 15 h	2.864	14.154	4.94	1.32	0.41

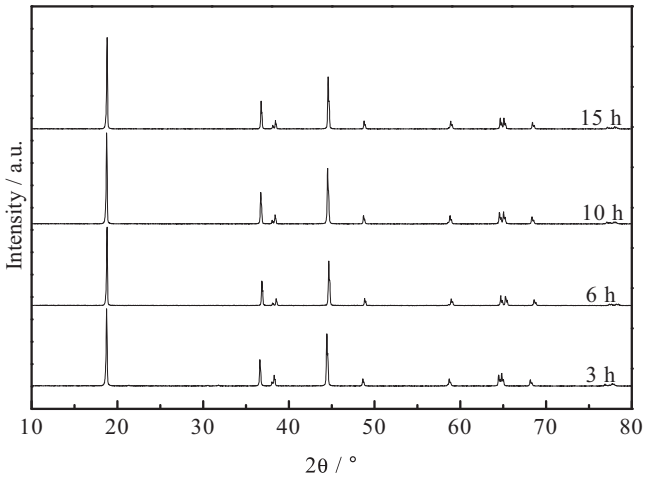

Fig. 4. XRD patterns of the $LiNi_{0.8}Co_{0.15}Al_{0.05}O_2$ samples sintered at 700 °C for various time.

(0 1 8)/(1 1 0). Table 1 lists the structural and lattice parameters calculated based on the X-ray diffraction patterns, where the R-factor indicates the $(I_{(0\,0\,6)}+I_{(0\,1\,2)})/I_{(1\,0\,1)}$ ratio, as defined by Reimers et al. [28]. Generally, higher values of the c/a and $I_{(0\,0\,3)}/I_{(1\,0\,4)}$ ratios are acknowledged as a less degree of cation mixing [29–31], and a lower R-factor value is recognized as a better hexagonal ordering structure [28,31]. As seen in Table 1, the sample calcined at 700 °C shows the highest c/a and $I_{(0\,0\,3)}/I_{(1\,0\,4)}$ ratios, and the lowest R-factor, indicating the least cation mixing and the best hexagonal ordering.

Fig. 4 shows the XRD patterns of the $LiNi_{0.8}Co_{0.15}Al_{0.05}O_2$ samples sintered at 700 °C for different time. The structural and lattice parameters are also listed in Table 1. As can be seen, as the calcination time extends, both the values of the c/a and $I_{(0\,0\,3)}/I_{(1\,0\,4)}$ ratios increase first then start to drop. While the R-factor value changes reversely. Nevertheless, the maxima of the c/a and $I_{(0\,0\,3)}/I_{(1\,0\,4)}$ ratios and the minimum of the R-factor value appear simultaneously for the sample calcined for 6 h, indicating that this material calcined at this time has the maximum ordering of hexagonal two-dimensional layer structure. From the above analyses of the XRD patterns, it can be concluded that the optimal temperature and time for the $LiNi_{0.8}Co_{0.15}Al_{0.05}O_2$ powders are 700 °C and 6 h, respectively.

3.3. SEM studies

Fig. 5(a) shows SEM image of the $Ni_{0.8}Co_{0.15}Al_{0.05}OOH$ precursor prepared by the co-oxidation-controlled crystallization method. It is obvious that $Ni_{0.8}Co_{0.15}Al_{0.05}OOH$ powders have spherical morphology in secondary particles and the estimated particle size is about 5–12 μm in diameter, while the primary particles are needle-like shaped and they are densely agglomerated in secondary forms. As shown in Fig. 5(b), the morphology and size of $LiNi_{0.8}Co_{0.15}Al_{0.05}O_2$ secondary particles calcined at 700 °C for 6 h remain almost the same as the precursor. However, it can be found easily that the needle-shaped primary particles of $Ni_{0.8}Co_{0.15}Al_{0.05}OOH$ seen in Fig. 5(a) change to the cylinder-shaped primary particles of $LiNi_{0.8}Co_{0.15}Al_{0.05}O_2$ observed in Fig. 5(b).

3.4. Oxidation state of Ni studies

The composition analysis of the sample synthesized at 700 °C for 6 h was conducted by ICP-AES. The molar ratio of Li:Ni:Co:Al was 1.010:0.801:0.151:0.049, close to the ideal stoichiometry. The oxidation state of nickel of these powders was +3.0 by the chemical titration in Ar atmosphere. Meanwhile, in the Ni 2p XPS spectrum of these powders as shown in Fig. 6, the dominating Ni $2p_{3/2}$ peak is at 856.0 eV, which corresponds to a Ni^{3+} [23]. In that XPS is surface sensitive with about 10 nm probing depth, Ni ions at the surface of $LiNi_{0.8}Co_{0.15}Al_{0.05}O_2$ powders exist as Ni^{3+}, which is different from literatures [32,33] that thought most Ni^{2+} ions appeared

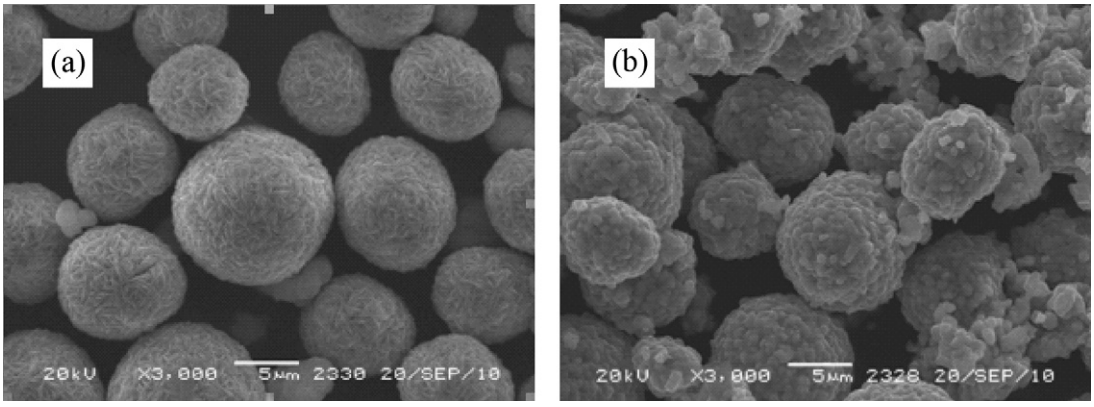

Fig. 5. SEM images of (a) $Ni_{0.8}Co_{0.15}Al_{0.05}OOH$ and (b) $LiNi_{0.8}Co_{0.15}Al_{0.05}O_2$ powders calcined at 700 °C for 6 h.

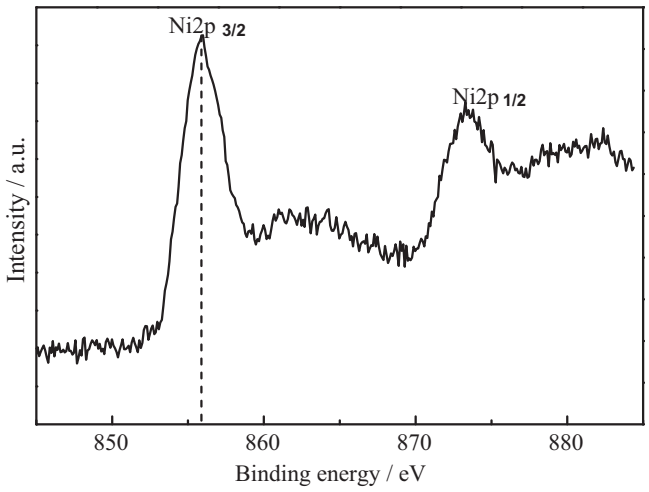

Fig. 6. The Ni 2p XPS spectrum of $LiNi_{0.8}Co_{0.15}Al_{0.05}O_2$ powders.

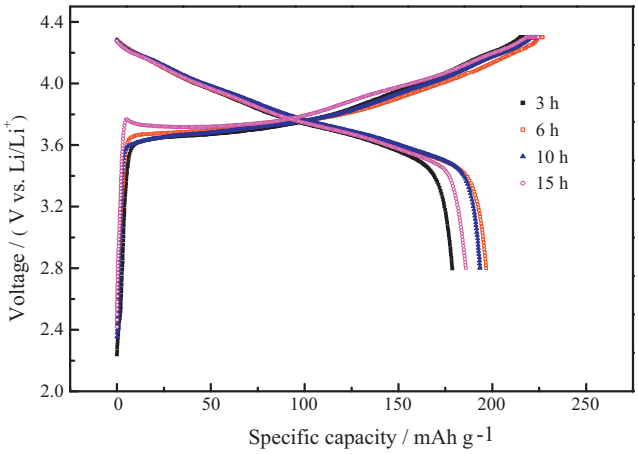

Fig. 8. The initial charge–discharge curves of the $LiNi_{0.8}Co_{0.15}Al_{0.05}O_2$ powders prepared at 700 °C for different time.

at the surface of $LiNi_{0.8}Co_{0.15}Al_{0.05}O_2$ powders. This difference maybe originates from using $Ni_{0.8}Co_{0.15}Al_{0.05}OOH$ as the precursor to prepare $LiNi_{0.8}Co_{0.15}Al_{0.05}O_2$ powders. The results again prove reduction of cation mixing which occurs between Li^+ and Ni^{2+} due to the difference of ionic radii ($r_{Ni^{3+}} = 0.56\,Å$, $r_{Ni^{2+}} = 0.70\,Å$, and $r_{Li^+} = 0.74\,Å$)[23].

3.5. Electrochemical properties

The initial cycle charge–discharge curves of the $LiNi_{0.8}Co_{0.15}Al_{0.05}O_2$ powders prepared at different calcination temperatures for 6 h are plotted in Fig. 7. The corresponding data of initial charge/discharge capacities and efficiencies are listed in Table 2. As can be seen, except the $LiNi_{0.8}Co_{0.15}Al_{0.05}O_2$ powders prepared at 600 °C, the discharge specific capacity values of other samples are more than 181 mAh g^{-1}, the efficiency values more than 82%. In particular, the sample calcined at 700 °C has an initial charge specific capacity of 226.7 mAh g^{-1}, and delivers a capacity of 196.8 mAh g^{-1} with an efficiency of 86.8%. These phenomena imply that 700 °C is the optimal calcination temperature which is consistent with the XRD data.

The initial cycle charge–discharge curves of the $LiNi_{0.8}Co_{0.15}Al_{0.05}O_2$ powders prepared at 700 °C for different calcination time are plotted in Fig. 8. The corresponding data of initial charge/discharge capacities and efficiencies are also listed in Table 2. As can be seen, although the calcination time is different, the charge specific capacity and efficiency values are very close with the range of 220.0–226.7 mAh g^{-1} and 81.2–86.8%, respectively. However, the discharge specific capacity values have obvious difference. From 3 to 6 h, the discharge specific capacity of corresponding sample increases from 178.7 to 196.8 mAh g^{-1}. Extending the calcination time up to 10 and 15 h decreases the discharge specific capacity to 193.5 and 186.0 mAh g^{-1}, respectively.

Fig. 9 displays the cycle performance of the $LiNi_{0.8}Co_{0.15}Al_{0.05}O_2$ powders prepared at different calcination temperatures for 6 h. Apparently, the sample prepared at 700 °C shows the best cyclic ability. The discharge specific capacity of this sample decreases from 196.8 to 189.1 mAh g^{-1} in the first 50 cycles with the loss rate about 0.08% per cycle. However, for the samples prepared at 600 °C, 650 °C, 750 °C and 800 °C, the loss rates are about 0.28%, 0.17%, 0.14% and 0.18% per cycle, respectively. These results are consistent with the XRD data, indicating that higher initial hexagonal ordering of the powders favors to remain this stable structure during repeated lithium insertion and extraction.

Fig. 10 exhibits the cycle performance of the $LiNi_{0.8}Co_{0.15}Al_{0.05}O_2$ powders prepared at 700 °C for different calcination time. It is easily found that the sample prepared for 6 h shows the best cyclic ability with the capacity retention of 96.1% after 50 cycles. However, for the samples prepared at 3 h, 10 h and 15 h, the capacity retentions are about 88.7%, 95.1% and

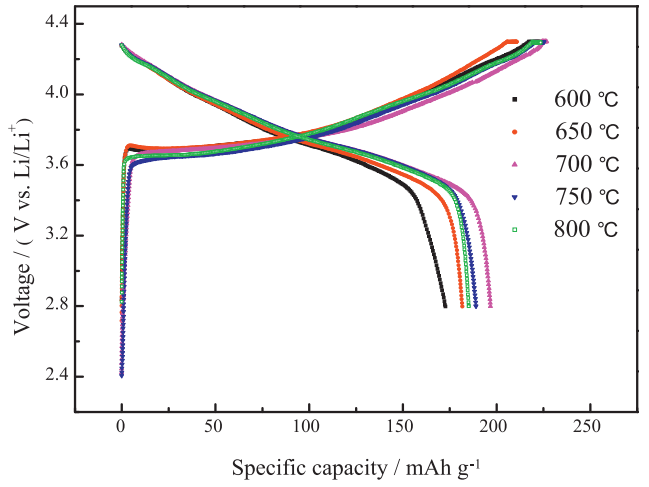

Fig. 7. The initial charge–discharge curves of the $LiNi_{0.8}Co_{0.15}Al_{0.05}O_2$ powders prepared at different temperatures for 6 h.

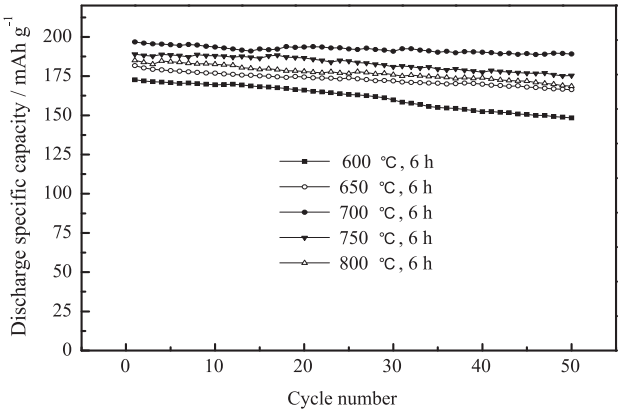

Fig. 9. Cycle performance of the $LiNi_{0.8}Co_{0.15}Al_{0.05}O_2$ powders prepared at different temperatures for 6 h.

Table 2
Initial charge/discharge specific capacities and efficiencies of $LiNi_{0.8}Co_{0.15}Al_{0.05}O_2$ samples sintered at various temperatures and time.

Reaction conditions	Charge specific capacity (mAh g^{-1})	Discharge specific capacity (mAh g^{-1})	Efficiency (%)
600 °C, 6 h	223.3	172.7	77.3
650 °C, 6 h	210.8	181.7	86.2
700 °C, 6 h	226.7	196.8	86.8
750 °C, 6 h	225.4	189.0	83.9
800 °C, 6 h	223.5	185.1	82.8
700 °C, 3 h	220.0	178.7	81.2
700 °C, 6 h	226.7	196.8	86.8
700 °C, 10 h	224.0	193.5	86.4
700 °C, 15 h	224.6	186.0	82.8

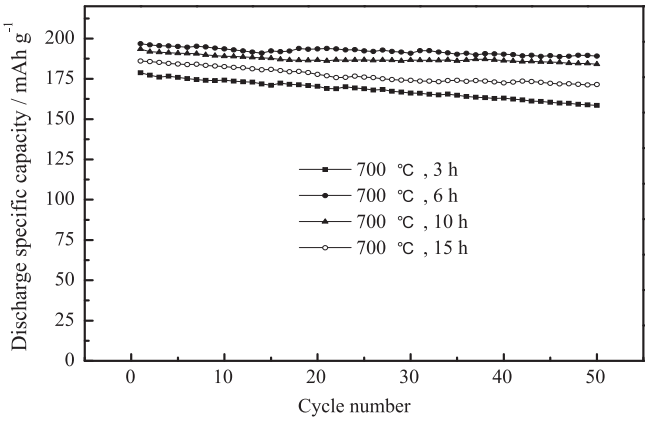

Fig. 10. Cycle performance of the $LiNi_{0.8}Co_{0.15}Al_{0.05}O_2$ powders prepared at 700 °C for different time.

92.2%, respectively. Again, the results prove that the excellent cyclic stability is attributed to the better layer structure and the particle morphology.

Fig. 11 presents the discharge specific capacities of the $LiNi_{0.8}Co_{0.15}Al_{0.05}O_2$ powders prepared at 700 °C for 6 h at rates of 0.1, 0.2, 0.5, 1.0 and 2.0 C. It is clear that the discharge capacities are stable at their own discharge rates, but capacity losses are larger at higher charge–discharge rates. This may be mainly related to the morphological change of particles and local structural changes of cathode material. These changes may be accelerated with increasing discharge rates [34].

Fig. 12 shows the cycle properties of the cathode powders prepared at 700 °C for 6 h at test temperature of 55 °C. The discharge capacity of the cathode powders was 194.6 mAh g^{-1} by the 50th cycle at a current density of 0.2 C. The discharge capacities of the

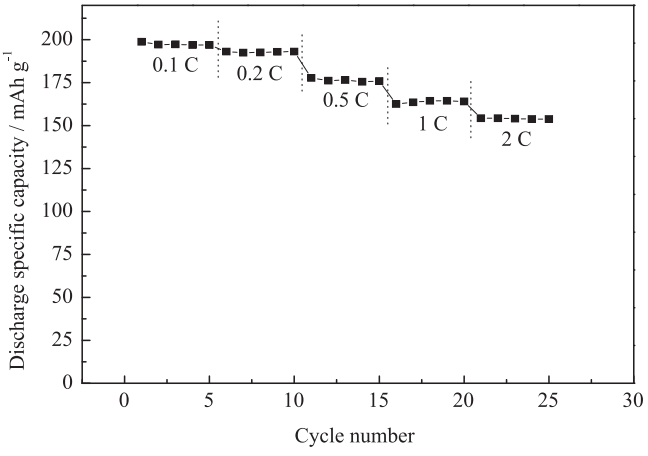

Fig. 11. Current density performance of the $LiNi_{0.8}Co_{0.15}Al_{0.05}O_2$ powders prepared at 700 °C for 6 h.

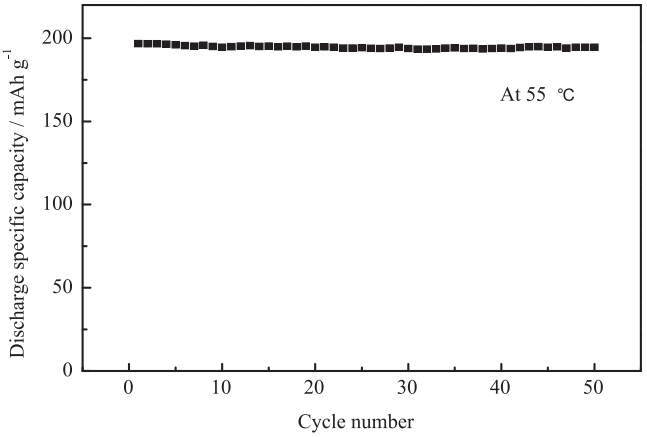

Fig. 12. Cycle performance of the $LiNi_{0.8}Co_{0.15}Al_{0.05}O_2$ powders prepared at 700 °C for 6 h at test temperature of 55 °C.

cathode powders at the high temperature of 55 °C are higher than those obtained at room temperature. The high discharge capacities of the cathode powders are due to the improved ion conductivity at elevated temperature [16].

4. Conclusions

$LiNi_{0.8}Co_{0.15}Al_{0.05}O_2$ cathode material was synthesized from the precursor $Ni_{0.8}Co_{0.15}Al_{0.05}OOH$ prepared by the co-oxidation-controlled crystallization method. The sample prepared by calcination at 700 °C for 6 h has the best electrochemical properties, with an initial discharge capacity of 196.8 mAh g^{-1} and capacity retention of 96.1% after 50 cycles when cycled at 0.2 C between 2.8 and 4.3 V, as well as excellent rate capability and high-temperature performance. This is due to excellent cationic ordering, hexagonal ordering and crystallinity, as well as spherical morphology and uniform particle size with diameter in the 5–12 μm range. Therefore, our method is an effective one to prepare the nickel-rich based cathode material with high discharge capacity and good cycle life.

Acknowledgments

This work was supported by the National Natural Science Foundation of China (No. 50604018) and the National Key Technology R&D Program of China (No. 2007BAE12B01).

References

[1] M.G.S.R. Thomas, W.I.F. David, J.B. Goodenough, P. Groves, Mater. Res. Bull. 20 (1985) 1137.
[2] S. Yamada, M. Fujiwara, M. Kanda, J. Power Sources 54 (1995) 209.
[3] T. Ohzuku, A. Ueda, M. Kouguchi, J. Electrochem. Soc. 142 (12) (1995) 4033.
[4] T. Ohzuku, T. Yanagawa, M. Kouguchi, A. Ueda, J. Power Sources 68 (1997) 131.
[5] J.R. Dahn, U.V. Sacken, M.W. Juzkow, H. Al-Janaby, J. Electrochem. Soc. 138 (1991) 2007.

[6] S. Madhavi, G.V. SubbaRao, B.V.R. Chowdari, S.F.Y. Li, J. Power Sources 93 (2001) 156.
[7] S. Madhavi, G.V. SubbaRao, B.V.R. Chowdari, S.F.Y. Li, Solid States Ionics 152–153 (2002) 199.
[8] C.H. Chen, J. Liu, M.E. Stoll, G.L. Henriksen, D.R. Vissers, K. Amine, J. Power Sources 128 (2004) 278.
[9] W.S. Kim, K. Chung, Y.K. Choi, Y.E. Sung, J. Power Sources 115 (2003) 101.
[10] H. Cao, B.J. Xia, N.X. Xu, C.F. Zhang, J. Alloys Compd. 376 (2004) 282.
[11] P. Kalyani, N. Kalaiselvi, N.G. Renganathan, M. Raghavan, Mater. Res. Bull. 39 (2004) 41–54.
[12] M. Guilmard, C. Pouillerie, L. Croguennec, C. Delmas, Solid State Ionics 160 (2003) 39.
[13] C.J. Han, J.H. Yoon, W.I. Cho, H. Jang, J. Power Sources 136 (2004) 132.
[14] S.B. Majumder, S. Nieto, R.S. Katiyar, J. Power Sources 154 (2006) 262.
[15] P.H. Duvigneaud, T. Segato, J. Eur. Ceram. Soc. 24 (2004) 1375.
[16] S.H. Ju, H.C. Jang, Y.C. Kang, Electrochim. Acta 52 (2007) 7286.
[17] E. Zhecheva, R. Stoyanova, R. Alcantara, P. Lavela, J.L. Tirado, Pure Appl. Chem. 74 (10) (2002) 1885.
[18] V. Bianchi, S. Bach, C. Belhomme, J. Farcy, J.P. Pereira-Ramos, D. Caurant, N. Baffier, P. Willmann, Electrochim. Acta 46 (2001) 999.
[19] V. Bianchi, D. Caurant, N. Baffier, C. Belhomme, E. Chappel, G. Chouteau, S. Bach, J.P. Pereira-Ramos, A. Sulpice, P. Wilmann, Solid State Ionics 140 (2001) 1.
[20] A. Rougier, I. Saadoune, P. Gravereau, P. Willmann, C. Delmas, Solid State Ionics 90 (1996) 83.
[21] M. Guilmard, A. Rougier, M. Grune, L. Croguennec, C. Delmas, J. Power Sources 115 (2003) 305.
[22] A. Rougier, P. Gravereau, C. Delmas, J. Electrochem. Soc. 143 (4) (1996) 1168.
[23] H.S. Liu, Y. Yang, J.J. Zhang, J. Power Sources 162 (2006) 644.
[24] W.M. Liu, G.R. Hu, Z.D. Peng, K. Du, Y.B. Cao, Q. Liu, Chin. Chem. Lett. 22 (9) (2011) 1099.
[25] G.X. Wang, S. Zhong, D.H. Bradhurst, S.X. Dou, H.K. Liu, J. Power Sources 76 (1998) 141.
[26] W. Li, J.C. Currie, J. Electrochem. Soc. 144 (1997) 2773.
[27] D.C. Li, Z.H. Peng, W.Y. Guo, Y.H. Zhou, J. Alloys Compd. 457 (2008) L1.
[28] J.N. Reimers, E. Rossen, C.D. Jones, J.R. Dahn, Solid State Ionics 61 (1993) 335.
[29] T. Ohzuku, A. Ueda, M. Nagayama, J. Electrochem. Soc. 140 (1993) 1862.
[30] Y.M. Choi, S.I. Pyun, S.I. Moon, Solid State Ionics 89 (1996) 43.
[31] L.F. Xiao, Y.Y. Yang, Y.Q. Zhao, X.P. Ai, H.X. Yang, Y.L. Cao, Electrochim. Acta 53 (2008) 3007.
[32] W.S. Yoon, K.Y. Chung, J. McBreen, D.A. Fischer, X.Q. Yang, J. Power Sources 174 (2007) 1015.
[33] D.P. Abraham, R.D. Twesten, M. Balasubramanian, J. Kropf, D. Fischer, J. McBreen, I. Petrov, K. Amine, J. Electrochem. Soc. 150 (11) (2003) A1450.
[34] Y. Itou, Y. Ukyo, J. Power Sources 146 (2005) 39.